Available online at www.sciencedirect.com

SCIENCE DIRECT®

Journal of Controlled Release 101 (2005) 163–173

journal of controlled release

www.elsevier.com/locate/jconrel

Mapping neutral microclimate pH in PLGA microspheres

Lei Li, Steven P. Schwendeman*

Department of Pharmaceutical Sciences, University of Michigan, Ann Arbor, MI 48019-1065, USA

Received 3 April 2004; accepted 7 July 2004
Available online 30 September 2004

Abstract

A quantitative ratiometric method based on laser scanning confocal microscopic imaging was developed to create a pixel-by-pixel neutral microclimate pH (5.8–8.0) map inside poly(lactic-co-glycolic acid) (PLGA) microspheres. The method was accurate to within ±0.2 pH units. PLGA microspheres with encapsulated bovine serum albumin and the pH-sensitive dye, SNARF-1® dextran (MW=10 kDa), were prepared by a water-in-oil-in-water solvent evaporation method. The imaging method was used to monitor the pH changes in PLGA microspheres with or without co-encapsulation of acid-neutralizing $MgCO_3$, and for three different microsphere sizes (2.0±0.3, 40±10 and 137±32 μm) during incubation under physiological conditions. The pH of microspheres was significantly higher with co-encapsulated base compared to base-free microspheres, whose microclimate pH was predominantly below the dye detection limit of pH=5.8. The small microspheres displayed a more neutral pH during incubation probably due to their much shorter diffusion path for polymer-dissolved acids compared with medium- and large-size microspheres. The pH mapping technique discussed here may be useful in routine formulation development and for elucidation of mechanisms of microclimate pH development and polymer erosion.

Keywords: Microclimate pH; PLGA microsphere; Laser scanning confocal microscope; Ratiometric imaging; Protein stability

1. Introduction

Despite the tremendously successful delivery of small, acid-stable peptides such as the luteinizing hormone-releasing hormone (LHRH)-agonists from poly(lactic-co-glycolic acid) (PLGA) delivery systems for treatment of prostate cancer [1,2], the delivery of proteins has been complicated by numerous destabilizing factors during microencapsulation, storage and release [3–5]. Among those protein-damaging stresses between microencapsulation and release, poor control of the pH in PLGA delivery systems has been implicated as one of the most significant [3,6–9]. It has long been recognized that the pH inside the aqueous pores of the PLGA matrix, i.e., the "microclimate pH" can become very acidic during bioerosion as a result of acidic polymer impurities and the hydrolysis of the PLGA polyester to form acidic monomers and oligomers [10]. As a consequence,

* Corresponding author. Tel.: +1 734 615 6574; fax: +1 734 615 6162.
E-mail address: schwende@umich.edu (S.P. Schwendeman).

0168-3659/$ - see front matter © 2004 Elsevier B.V. All rights reserved.
doi:10.1016/j.jconrel.2004.07.029

many encapsulated drugs that cannot withstand such a low pH (e.g., pH~2 reported by Herrlinger [11]) are rapidly degraded during bioerosion of PLGAs.

Two common configurations, microspheres (1–100 μm, e.g., the Lupron Depot [12], Takeda Chemical) and millicylinders (cylindrical rods of 0.8–1.5 mm diameter, e.g., the Zoladex implant [1], AstraZeneca Pharmaceuticals) are currently used and the microclimate in both has been shown ubiquitously acidic. However, only recently has it been demonstrated that acid-labile molecules of all kinds including anticancer drugs, angiogenic proteins and vaccine antigens can all be stabilized in PLGA delivery systems when novel techniques are used to raise the acidic pH in the PLGA matrix to neutral values [5,9,13,14]. For example, the use of antacid excipients, such as $Mg(OH)_2$, $MgCO_3$ and $ZnCO_3$, have conferred stability to encapsulated vincrinstine, basic fibroblast growth factor and the tetanus vaccine antigen [9,13,15]. Therefore, it is essential to develop methods to quantitatively measure, predict and control the microclimate pH in such delivery systems if this novel finding is to become generally applicable.

Previous methods to measure microclimate pH in PLGA include (1) ensemble average measurements using electron paramagnetic resonance (EPR) [16,17], nuclear magnetic resonance (NMR) [18] and potentiometry; and (2) direct visualization techniques, such as confocal imaging of pH sensitive dyes [8,14]. In the EPR method, the constant of hyperfine splitting, 2aN, was used to determine an average pH inside PLGA microspheres. Because the experiments relied on the mobility of spin-labeled protein, with an increase of the microviscosity in the later hours of the experiments, the spectra of EPR was changed and signal-to-noise ratio decreased to prevent the measurement of pH throughout the release period [16]. The potentiometric measurements can give rapid values of pH for thin polymer films, and the pH of the thin water film between the electrode and polymer mimics the microclimate pH of aqueous pores inside the polymer drug delivery system. However, it is difficult to mimic microclimate pH of a small-scale system, such as microspheres or nanospheres, which may have unique microstructures, excipient/drug distributions and transport characteristics. Overall, the ensemble average measurements described above could give a general picture of microclimate pH at the macroscopic level. However, the microscopic level of the detection can only be achieved through direct visualization techniques, such as microscopic imaging.

Shenderova and Burke [14] first developed the confocal microscope imaging method to relate the microclimate pH with the fluorescent intensity. Because of the difficulty of control and predict the fluorescein concentration in the aqueous pore inside the microsphere, the method was only semi-quantitative. Fu et al. [8] improved the confocal microscopic imaging method by co-encapsulating two dextran-fluorescent dyes conjugates inside microspheres and related the ratio of the two dye images with microclimate pH in order to eliminate the poorly controlled effects of dye concentration and pore distribution. However, both of the dyes emit in the green range (535 nm for NERF and 580 nm of SNARF), giving rise to poor resolution without a narrow bandwidth detector. Because of the high noise-to-signal ratio from the ratio images, the prediction of pH is also expected to be semi-quantitative.

In order to overcome the aforementioned drawbacks in microclimate pH measurement, a new quantitative ratiometric method based on laser scanning confocal microscopic imaging was developed to create a pixel-by-pixel neutral range microclimate pH map inside PLGA microspheres. This method was then applied to both acid-neutralized and non-neutralized PLGA microspheres during extended incubation in physiological buffer.

2. Materials and methods

2.1. Chemicals

Poly(D,L-lactic-co-glycolide) with inherent viscosity equal to 0.19 dl/g in methylene chloride at room temperature was generously provided by Alkermes (Cambridge, MA). The fluorescent pH sensitive dye, SNARF-1® dextran (MW=10 kDa), was from Molecular Probes (Eugene, OR); bovine serum albumin (BSA, fraction V) was purchased from Sigma (St. Louis, MO); poly(vinyl alcohol) (PVA, 9−10 kDa, 80% hydrolyzed) was from Polysciences (Warrington, PA); and $MgCO_3$ was from Sigma. All other solvents, acids and bases

were obtained from Fisher Scientific, and all reagents and buffer salts were obtained from Sigma. Distillated and deionized water used in this study was obtained from a Barnstead NANOpure Diamond™ Ultrapure Water Systems (Dubuque, IA).

2.2. Microsphere preparation

PLGA microspheres were prepared by a w/o/w double emulsion-solvent evaporation microencapsulation method [9]. The formulation parameters to achieve small, medium and large microspheres are listed in Table 1. In brief, 130 μl of 150–200 mg/ml BSA with 2–3 mg/ml SNARF-1 dextran in PBS solution was added to a 500–700 mg/ml polymer in CH_2Cl_2 solution with or without 3% w/w of $MgCO_3$. The mixture was homogenized at 15,000 rpm (Virtis IQ^2, Gardiner, New York) in an ice/water bath for 1.5 min to make the first emulsion. Two milliliters of 2–10% PVA solution were immediately added to the first emulsion and the mixture was homogenized at 15,000 rpm or vortexed for 1 min to make the w/o/w emulsion. The final emulsion was then poured into 100 ml of 0.5% PVA solution under stirring and hardened for 3 h at room temperature. The hardened microspheres were then sieved and collected by centrifugation and washed three times with water before lyophilization on a Labconco freeze dryer (Kansas City, CO) for 48 h. In one case, where a three-dimensional microclimate pH map was performed, we used a lower BSA loading (135 μl of 70 mg/ml BSA in 500 mg/ml polymer solution), and a lower homogenized speed of 10,000 rpm for the first emulsion. All other conditions were as described above.

Table 1
Summary of microsphere preparation conditions

Size	Diameter (μm)	Polymer concentration[a] (mg/ml)	Homogenization speed[b] (rpm)	PVA (w/v)
Small	2	500	15,000	10%
Medium	40	500	15,000	2%
Large	137	700	votex	2%
Small for 3D imaging	10	500	10,000	5%

[a] The polymer used in all formulations was PLGA 50/50, i.v.=0.19 dl/g.
[b] The homogenization speed was used for preparation of the w/o/w emulsion.

2.3. Microsphere size distribution by scanning electron microscopy

PLGA microspheres were first coated with a 10-nm layer of Au–Pd using Hummer VI Sputter Coater (Anatech). The morphology of the microspheres was then observed by a scanning electron microscope (Philips XL30FEG, FEI). The accelerating voltage was set at 3 keV. 70–140 microspheres were measured to determine the size distribution of each microsphere preparation.

2.4. Confocal imaging of microclimate pH inside PLGA microspheres

A ratiometric method based on imaging with a laser scanning confocal microscope (LSCM, Leica TCS SP2) was developed to map the microclimate pH inside microspheres. The fluorescent dye that was encapsulated in the microspheres was excited at 488 nm by an Ar/He laser, and two images at different wavelengths (580 and 640 nm) were taken; the ratio image I_{640}/I_{580} was correlated with pH from a standard curve independent of dye concentration. An image at a wavelength corresponding to the isosbestic point (pH-insensitive) of the dye was also examined to estimate the concentration of the dye. All measurements were conducted using a 63× oil immersion objective with numerical aperture of 1.4.

2.5. Image processing for pH map

To eliminate the white noise from the detector, image processing steps are critical to obtain a pixel-by-pixel pH map within a reasonable error range. Hence, we evaluated each image processing procedure by checking the distribution of the fluorescent intensity, intensity ratio distribution and corresponding pH distribution from standard pH solutions. By fitting the distribution curve with a Gaussian distribution function, the standard deviation and the standard error of the mapping was obtained and served as the criteria of choosing the appropriate image processing steps. We examined four different image processing algorithms [19]: (1) frame averag-

ing (FA), which eliminates the white noise of the signal assuming that the structure of the imaged specimen does not change during the time of measurement; (2) and (3) neighborhood averaging (NA) and applying a median filter (MF), which eliminates the signal noise assuming that the spatial resolution is adequate for important details; and (4) threshold (TH), which eliminates the fluorescent effect from release media and measures only the image detail in the concentration range from the standard curve.

The overall procedure of image processing is summarized in Table 2. First, the fluorescent images from three different wavelengths were read into three corresponding two-dimensional matrices, r_{ij} (580 nm), g_{ij} (640 nm) and I_{ij} (610 nm). Then, each image-processing algorithm was used, and the new signal distribution was fit with a Gaussian distribution, and the corresponding standard deviation was obtained. By using a standard curve obtained from fixed pH solutions, the pixel-by-pixel pH was then obtained.

Table 2
Image processing steps and algorithms

Steps	Procedures
1	Read in image from channel 1 (580 nm), r_{ij}; i, j represent the coordinate of the pixel
2	Read in image from channel 2 (640 nm), g_{ij}
3	Read in image from channel 3 (610 nm), I_{ij}
4	Frame averaging, average signals through all frames for r_{ij} and g_{ij} $r(i,j)=\frac{\sum_{k=1}^{nf} r_k(i,j)}{nf}$; $g(i,j)=\frac{\sum_{k=1}^{nf} g_k(i,j)}{nf}$; nf is number of frames
5	Neighborhood averaging, $P^*_{x,y}=\frac{\sum_{i,j=-m}^{+m} w_{ij}P_{x+i,y+j}}{\sum_{ij=-m}^{+m} w_{i,j}}$; P represents matrix r or g, and P^* is the new matrix of r or g after neighborhood averaging; w is a weighting matrix, as follows: $w=\begin{bmatrix}1&2&1\\2&4&2\\1&2&1\end{bmatrix}$.
6	Median filter, a convolution operation with intensity matrix, and the kernel size.
7	Generate ratio image: if I_{ij}>threshold, $R_{ij}=\frac{g_{ij}}{r_{ij}}$; if I_{ij}<threshold, $R_{ij}=0$;
8	Fit R_{ij} probability density function according to a Gaussian distribution: $I=\frac{1}{\sqrt{2\pi}\sigma}e^{-\frac{(R-R_0)^2}{2\sigma^2}}$; I is the probability density function of R_{ij}, R_0 is the average of R_{ij}, σ is the standard deviation of R_{ij}
9	Calculate pH pixel by pixel using R_{ij} and standard curve
10	Calculate pH distribution

2.6. Calibrating fluorescent intensity ratio with pH

The standard curve of pH vs. fluorescent intensity ratio was determined using 0.1 M sodium phosphate buffer solutions from pH 5.8 to 8.0 with SNARF-1 dextran concentrations of 0.8, 1.0 and 2.0 mg/ml.

2.7. Microclimate pH mapping inside PLGA microspheres

Ten milligrams of microspheres were suspended in 1 ml phosphate buffer saline plus 0.02% Tween 80 pH=7.4 (PBST) under mild agitation at 37 °C. At predetermined times, the release media was removed after mild centrifugation (3 min at 2000×g) and fresh buffer was added to maintain sink conditions. At the same time, a small amount of microspheres was removed to obtain confocal images for microclimate pH mapping.

3. Results and discussion

3.1. Confocal imaging of microclimate pH inside PLGA microspheres

The fluorescent probe, dextran-SNARF-1® conjugate, was encapsulated with protein (BSA) in order to map the microclimate pH inside microspheres. The protonation of SNARF-1 phenolic substituent as pH is increased results in its emission spectrum undergoing a shift to longer wavelength. This pH dependence allows the ratio of the fluorescent intensities from the dye at two emission wavelengths, typically 580 and 640 nm, to be used for quantitative determinations of pH. The high molecular weight dextran conjugation can inhibit the dye leaching out from the specimen, such as microspheres, and localize the dye in the aqueous pores similar to the partition behavior of proteins in the polymer [8]. This dye is useful to sense pH within the neutral pH range.

The advantage of the SNARF-1 emission spectral shift is the use of the ratio of relevant intensities (580 and 640 nm) to cancel artifactual variations in the fluorescence signal that might otherwise be misinterpreted as changes in ion concentration [20]. In addition to their indicator concentration independence, ratiometric measurements reduce or eliminate variations of several other determining factors in the measured

fluorescence intensity including excitation path length, excitation intensity and detection efficiency. Therefore, the ratiometric method can also eliminate artifacts including photo-bleaching, leakage of the indicator, variable cell thickness and non-uniform indicator distribution within a microsphere or among populations of microspheres (due to loading efficiency variations). Whereas the fluorescence lifetime measurement is generally considered most rigorous, the ratiometric method has an easy and simple setup, which is applicable for routine use in formulation research.

3.2. Image processing

Without image processing of the fluorescent intensity signal from the LSCM, the mapped pH can have an unacceptably board spectrum. A good image processing strategy can improve the signal/noise ratio dramatically and result in a narrow Gaussian distribution of pH map with a reasonably low standard error.

An example to show the result of image processing from a standard phosphate buffer solution at pH=7.4 is displayed in Fig. 1. The pH distributions from the standard solution became more narrowly distributed after each step of the processing. Table 3 lists the averaged mapped pH and the standard error after each step of image processing. All image-processing steps (FA, NA and MF) were essential to obtain a reliable pH map. By checking the intensity distribution of each channel image, distribution of ratio image and pH distribution of mapped image from standard solution, we observed the following: (i) with ≥6-frame averaging steps, the intensity distribution of the channel image became Gaussian; (ii) ≥20-frame averaging steps alone, or with 6-frame averaging steps plus neighborhood averaging, the intensity distribution of the ratio image became Gaussian; and (iii) with 20-frame averaging steps, plus neighborhood averaging, plus applying the median filter, the pH distribution of the mapped image became Gaussian. Hence, in our pH mapping method, we selected the most rigorous processing algorithm (averaged 20 frames, plus neighborhood averaging and median filter application). The mapped pH and standard error of all standard pH solutions are listed in Table 4. With the proposed image processing technique, we were able to accurately map the pH within the range of ±0.12 over an appreciable pH range, provided we maintain the probe concentration within the desired concentration interval (e.g., 0.8–2 mg/ml, also see below).

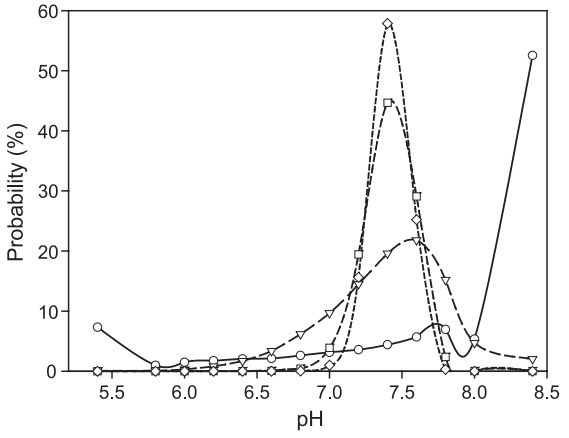

Fig. 1. pH distribution with different image processing methods. Processing methods include: one frame without image processing (○), 20-frame averaging (▽), 20-frame averaging with neighborhood averaging (□), and 20-frame averaging plus neighborhood averaging and median filter (◇).

Table 3
pH distribution of PBS pH 7.4 after different image processing techniques

	1 frame	20 frames[a]	20 frames NA[b]	20 frames NA MF[c]
Mean pH	8.38	7.47	7.43	7.42
S.E.M.[d]	1.25	0.38	0.17	0.14

[a] Averaged over 20 frames.
[b] Neighborhood averaging was performed following frame averaging.
[c] Median filter was applied after neighborhood averaging.
[d] Standard error of the mean.

3.3. Development of the standard curve

The standard curve of pH vs. intensity ratio was determined using standard pH buffer solutions of pH 5.8–8.0 with dye concentrations of 0.8, 1.0 and 2.0 mg/ml, as seen in Fig. 2. From the standard curve, a concentration independent range was verified between 0.8 and 2.0 mg/ml, and the pH sensitive range of the dye was roughly 5.8–8.0. As mentioned in the previous section, the fluorescent image near the isosbestic point, 610 nm, was also taken in order to detect the probe concentration. As seen in Fig. 3, the fluorescent intensities of pH buffer solution had little

Table 4
Standard error for different pH and dye concentration after image processing[a]

pH		5.8	6	6.2	6.4	6.6	6.8	7	7.2	7.4	7.6	7.8	8
1.0 μg/ml	err+[b]	0.097	0.093	0.092	0.087	0.081	0.073	0.066	0.057	0.049	0.041	0.035	0.031
	err−	−0.115	−0.111	−0.110	−0.106	−0.101	−0.091	−0.085	−0.076	−0.067	−0.057	−0.048	−0.038
2.0 μg/ml	err+	0.091	0.089	0.084	0.074	0.068	0.062	0.054	0.045	0.037	0.031	0.031	0.042
	err−	−0.106	−0.104	−0.100	−0.088	−0.083	−0.077	−0.070	−0.060	−0.051	−0.041	−0.032	−0.033

[a] The image was processed using 20-frame averaging, neighborhood averaging, plus applying median filter.
[b] err+/err− was determined by the standard deviation of fitted Gaussian distribution of intensity ratio, number of pixels measured, and corresponding position at the pH standard curve.

variation in the pH 5.8–8.0 range (especially for the highly relevant range of 5.8–7.0, see below), but changed significantly with probe concentration. Hence, the upper (2 mg/ml) and lower (0.8 mg/ml) curves served as the criteria for prediction of pH in the desired probe concentration interval.

3.4. pH mapping in PLGA microspheres

The microclimate pH mapping inside PLGA microspheres with and without $MgCO_3$ base particles was investigated as a function of incubation time (2 h to 35 days) and size of the microspheres (2, 40 and 137 μm mean diameter). The pH distribution among microspheres with and without base was also determined. These results are described below. Since the probe is dissolved in aqueous pores, and not in the polymer phase, in the hydrated microsphere matrix, we assumed that similar absorption/emission behavior from the dye between the test microspheres and the standard solutions was recorded.

3.4.1. Small-size microspheres

In the presence of base, at the initial stage (2 h after incubation), the microspheres were mostly in the detectable range (pH=5.8–8.0) and the average pH was ~6.4 (see Fig. 4A). With increasing incubation time, the microspheres became steadily more acidic. By 7 days, inside the microspheres 40% of the pores were below the detection limit of pH 5.8. Then, by 21 days of incubation, the pH decreased slightly, but remained mostly constant (for pH values in the observable range). At the 35-day endpoint, the pH kept decreasing and about 55% of the pores were below the detection limit. From the pH map in Figs. 5A–C, the pH inside the microspheres was not uniformly distributed, especially after a long time of

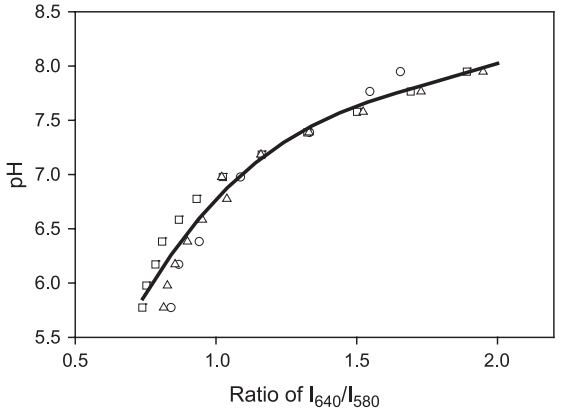

Fig. 2. Standard curve for dextran SNARF-1 conjugate (MW= 10,000 Da) at three different dye concentrations, namely 0.8 mg/ml (○), 1.0 mg/ml (□) and 2.0 mg/ml (△). A third order polynomial was fit to the data (r^2=0.9705).

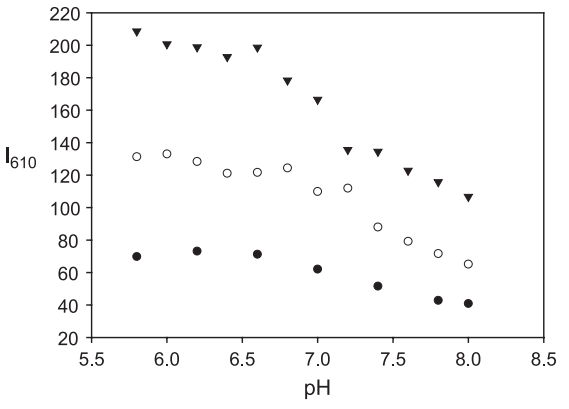

Fig. 3. Fluorescent intensity at isosbestic point, 610 nm, for three different dye concentrations (0.8 mg/ml (●), 1.0 mg/ml (□) and 2.0 mg/ml (▼)) in standard buffer solutions.

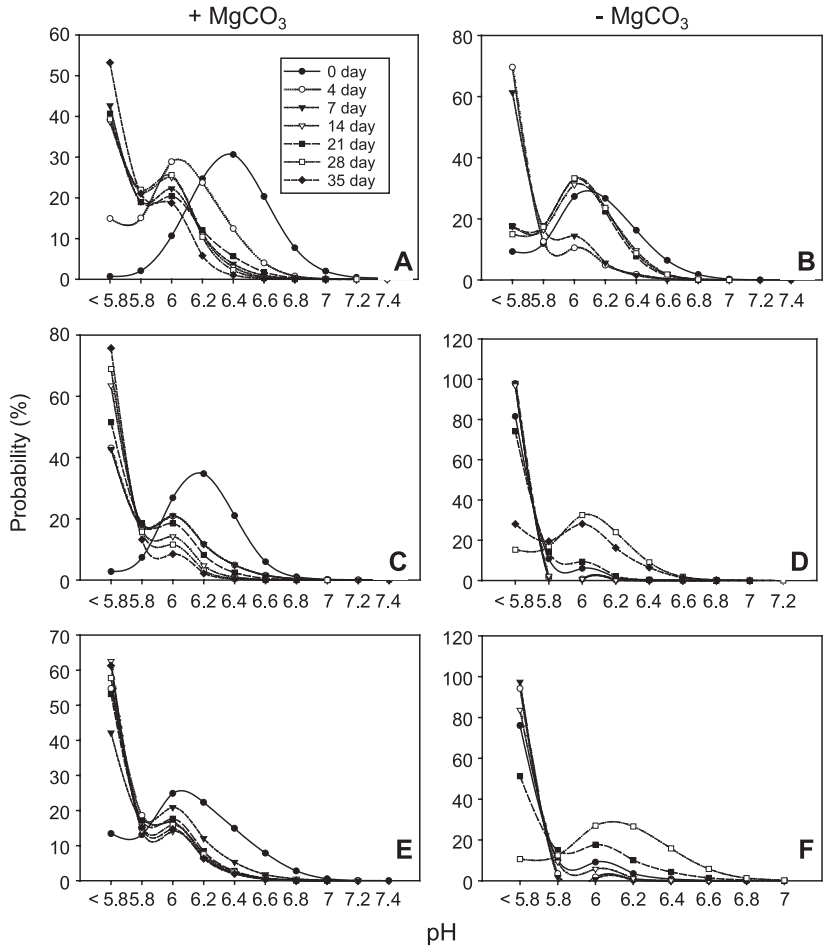

Fig. 4. pH distribution of small, medium, and large PLGA microspheres in the presence (A), (C) and (E) or absence (B), (D) and (F) of 3% $MgCO_3$ at different time points (2 h (●), 4 day (○), 7 (▼), 14 (▽), 21 (■), 28 (□) and 35 (♦) days).

incubation. The pH in pores at the edge of the microspheres was more neutral than those pores found close to the center. Likewise, as noted previously [14], regions of the microspheres surrounding the location of base particles were found to be a more neutral pH than those base-free regions.

For the non-base microspheres, at the initial stage, most of the pores were in the detectable range with only 10% below the detection limit (pH 5.8) and the average pH was around 6, which was lower than observed for base-containing microspheres (see Fig. 4B). The first week was the most acidic period during incubation and about 65–70% of the microspheres was below the detection limit. After 14 days of incubation, the pH began to rise. The pH shifted to the neutral range by 21 days and its distribution was similar to that at the initial stage with an average pH of ~6. Again, the pH was higher near the microsphere edge (see Figs. 5D, E and F), since the microspheres are suspended in the PBST buffer solution with pH=7.4. The water-soluble acids generated by the PLGA hydrolysis were likely able to diffuse out close to the edge of the microspheres.

3.4.2. Medium-size microspheres

In the presence of base, at the initial stage (2 h after incubation), the microspheres had an average

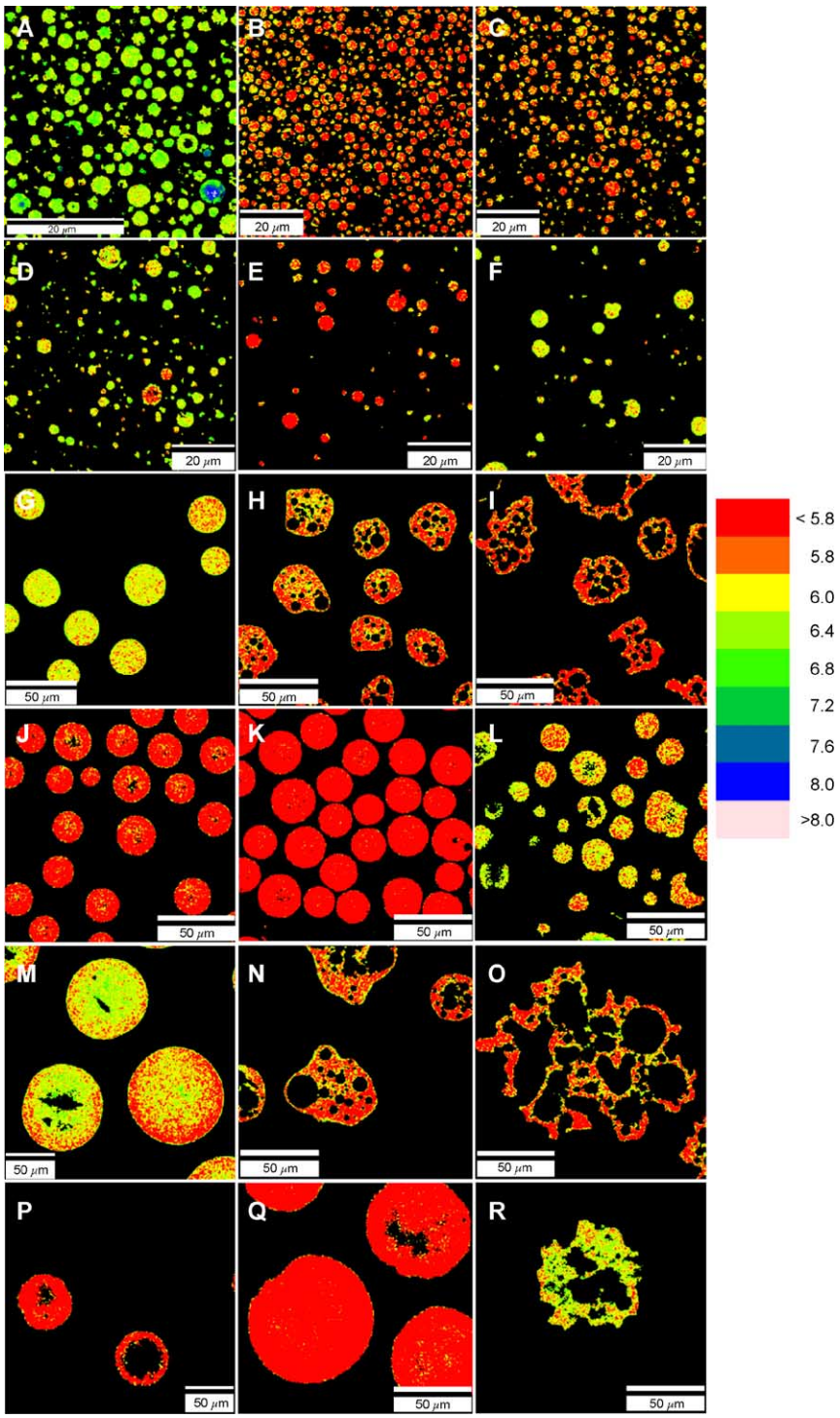

Fig. 5. pH map of small PLGA 50/50 microspheres with and without base at different incubation times (2 h, 7 days and 28 days). (A, B, C) Small-size microspheres with base, (D, E, F) small-size microspheres without base, (G, H, I) medium-size microspheres with base, (J, K, L) medium-size microspheres without base, (M, N, O) large-size microspheres with base and (P, Q, R) large-size microspheres without base.

observable pH of 6.2 (see Fig. 4C) and the pH was mostly in the detection range (pH=5.8–8.0). With increasing incubation time, the pH of microspheres decreased. By the 35-day endpoint, about 75% of the pores were below the detection limit of pH 5.8. We can see that after incubation for 7 days, large aqueous pores became noticeable, which appeared as black "holes" in the pH map with apparently no fluorescent dye present (Fig. 5H). In addition, pores became steadily more connected, which appeared to facilitate the release of the dye (Fig. 5I). Because of the "generation" of these large pores inside PLGA microspheres, the microspheres were swollen significantly compared with those in the initial stage (Figs. 5G and I). Swelling is a well-known consequence of antacid addition to PLGA [9,21].

For the non-base microspheres, at the initial stage, over 80% of the pores were below the detection limit (pH 5.8, see Fig. 4D). Then, during the first 2 weeks of incubation, almost all the pores fell below pH 5.8. By 21 days, the pH inside microspheres started to increase and reached a level similar to the initial stage. By 28 days, the pH distribution showed a Gaussian distribution with an average of pH=6.0. These non-base microspheres did not appear to swell significantly during the incubation, and little new large aqueous pores can be observed from the images (see Figs. 5J, K and L). By the 35-day end-point, the microspheres had already lost their integrity.

3.4.3. Large-size microspheres

In the presence of base, at the initial stage, the average observable pH inside the microspheres was close to 6.0 (see Fig. 4E) and about 15% of the pores were below the detection limit of pH 5.8. During incubation, the microspheres became steadily more acidic. By the end-point of 35 days, over 60% of the pores were below the detection limit. The pH map in Figs. 5M, N and O did not only give the pH distribution inside microspheres, but also illustrated the morphology changes of the microspheres. Due to the generation of large pores in the very early stage of the incubation (see Fig. 5N, for 7-day incubation), the shapes of the microspheres changed significantly. These pH mapping images also indicated the aqueous pore growth dynamics inside microspheres. In Figs. 5N and O, it can be clearly seen that the pores grew from small to large and coalesced with the neighborhood pores. By the end of the incubation, the volumes of the microspheres were largely increased from the initial stage.

For the non-base microspheres, more than 75% of the pores were lower than the detection limit of pH 5.8 (see Fig. 4F). During the first week of incubation, the pH immediately decreased and over 95% of the pores were below pH 5.8. By 14 days, the pH began to increase and, by 28 days, an average pH of little over 6.0 was observed. Hence, the acidic environment catalyzes the degradation of the PLGA and, once degradation passes some characteristic time (e.g., the indication time to mass loss), the pH begins to increase back to the neutral range. The pH mapping images showed that at the initial stage, the total hydration of the large microspheres could not be achieved completely in 2 h, so that the fluorescent intensity in the center of the microspheres was very weak, and the pH could not be detected (Fig. 5P). The pH images also indicate that the morphology of the microspheres did not change significantly until the end of the incubation when PLGA microspheres started to lose their integrity (see Figs. 5P, Q and R).

3.5. The pH in the release media

In Fig. 6, pH values of the release media for 3 different sizes of microspheres with encapsulated $MgCO_3$ are displayed. It is clear that the pH changes in the release media had a significant lag and yet a much higher pH than the microclimate pH observed inside microspheres. For example, in the first week the pH of all three sizes of microspheres decreased from a little over 6 to more than 50% of the pores out of the detection limit (pH=5.8). Then, the pH decreased continually, but was more stable. In contrast, the pH in the release media did not change from 7.2 for about a week, then began to decrease, especially fast from the fourth to fifth week, and reached an absolute minimum value of pH=6 throughout the course of the experiments. However, both the pH and microclimate pH showed that pH was affected by the microsphere size. The larger the microspheres, the lower the observed pH.

3.6. Three-dimensional pH map of microspheres

With a series of "thin slice" images of microspheres, we used NIH ImageJ to reconstruct the

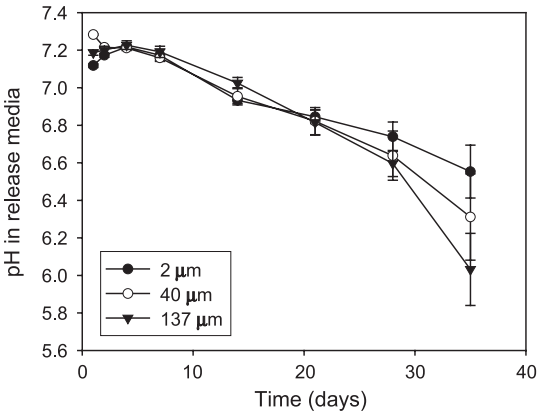

Fig. 6. pH of release media for small (●)-, medium (○)- and large (▼)-size microspheres with 3% $MgCO_3$.

original images and pH mapping images to obtain 3D images of a batch of microspheres containing larger pores than those previously described due to lower homogenization speed to produce the first emulsion (as described in Section 2). Fig. 7 shows the three-dimensional images projected in the horizontal direction. Fig. 7A and C is from the original image at wavelength of 580 nm; Fig. 7B and D is corresponding pH mapping images. Each aqueous pore and pH can be clearly seen. Moreover, we are currently evaluating the potential for porosity estimation from the 3-D images.

4. Conclusions

A method to map the pH in aqueous polymer pores based on ratiometric imaging with a laser scanning confocal microscope has been successfully developed. The method has been applied to the microclimate pH determination in PLGA microspheres. The pixel-by-pixel resolution of pH clearly demonstrates quantitative differences in microclimate pH as a function of three different sizes of microspheres during incubation under physiological conditions. The pH distributions are easily obtained from the pH images. The pH maps

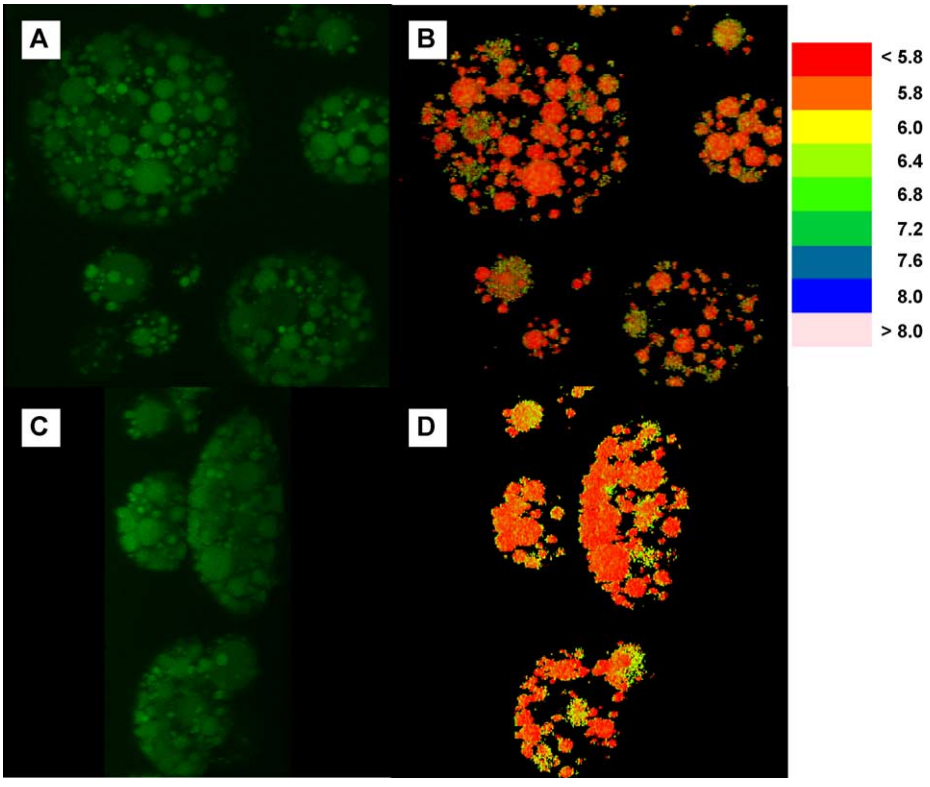

Fig. 7. Three-dimensional projection of microspheres: (A, C) projections of images at 580 nm and (B, D) projections of pH map images.

for the incubated acid-neutralized and non-neutralized microspheres gave clear indication that the microclimate inside PLGA microspheres can be much more acidic than the outside release media even when microspheres are as small as 2 μm in diameter. Hence, controlling the microclimate pH is a very important challenge to stabilize drugs inside drug carriers and this method should have application in formulation development and studies to elucidate the mechanism of microclimate pH kinetics. The incorporation of the base clearly increased pH in most instances, although the full impact of the base on pH in the microsphere specimens presented here will await further imaging using an additional acidic probe to compliment the pH range of SNARF-1.

Acknowledgements

This project was supported by NIH HL 68345. The authors give special thanks to Dr. Micheal J. Solomon (Dept. of Chemical Engineering, University of Michigan) for the use of confocal microscope, which is under the support of NSF CTS 0116331.

References

[1] F.G. Hutchinson, B.J.A. Furr, Biodegradable polymer systems for the sustained-release of polypeptides, J. Control. Release 13 (1990) 279–294.
[2] H. Toguchi, Pharmaceutical manipulation of leuprolide acetate to improve clinical performance, J. Int. Med. Res. 18 (1990) 35–41.
[3] S.P. Schwendeman, M. Cardamone, M.R. Brandon, A. Klibanov, R. Langer, The stability of proteins and their delivery from biodegradable polymer microspheres, in: S. Cohen, H. Bernstein (Eds.), Microparticulate Systems for the Delivery of Proteins and Vaccines, Marcel Dekker, New York, 1996, pp. 1–49.
[4] S.D. Putney, F.A. Burke, Improving protein therapeutics with sustained-release formulations, Nat. Biotechnol. 16 (1998) 153.
[5] S.P. Schwendeman, Recent advances in the stabilization of proteins encapsulated in injectable PLGA delivery systems, Crit. Rev. Ther. Drug Carr. Syst. 19 (2002) 73–98.
[6] S.P. Schwendeman, H.R. Costantino, R.K. Gupta, R. Langer, Peptide, protein, and vaccine delivery from implantable polymeric systems, in: K. Park (Ed.), Controlled Drug Delivery, ACS, Washington, DC, 1997, pp. 229–267. K. Park, ed.
[7] K. Fu, A.M. Klibanov, R. Langer, Protein stability in controlled-release systems, Nat. Biotechnol. 18 (2000) 24–25.
[8] K. Fu, D.W. Pack, A.M. Klibanov, R. Langer, Visual evidence of acidic environment within degrading poly(lactic-co-glycolic acid) (PLGA) microspheres, Pharm. Res. 17 (2000) 100–106.
[9] G. Zhu, S.R. Mallery, S.P. Schwendeman, Stabilization of proteins encapsulated in injectable poly(lactide-co-glycolide), Nat. Biotechnol. 18 (2000) 52–57.
[10] C.G. Pitt, M.M. Gratzl, G.L. Kimmel, J. Surles, A. Schindler, Aliphatic polyesters: II. The degradation of poly(DL-lactide), poly(e-caprolactone), and their copolymers in vivo, Biomaterials 2 (1981) 215–220.
[11] M. Herrlinger. PhD thesis, University of Heidelberg, Heidelberg, 1994.
[12] H. Okada, One- and three-month release injectable microspheres of the LH-RH superagonist leuprorelin acetate, Adv. Drug Deliv. Rev. 28 (1997) 43–70.
[13] J. Marinina, A. Shenderova, S.R. Mallery, S.P. Schwendeman, Stabilization of Vinca Alkaloids encapsulated in poly(lactic-co-glycolic acid) microspheres, Pharm. Res. 17 (2000) 677–683.
[14] A. Shenderova, T.G. Burke, S.P. Schwendeman, The acidic microclimate in poly(lactide-co-glycolide) microspheres stabilizes camptothecins, Pharm. Res. 16 (1999) 241–248.
[15] W.L. Jiang, S.P. Schwendeman, Stabilization of tetanus toxoid encapsulated in PLGA microspheres, Proceed. Int'l. Symp. Control. Rel. Bioact. Mater. 29 (2002) abstract #142.
[16] K. Mader, B. Bittner, Y. Li, W. Wohlauf, T. Kissel, Monitoring microviscosity and microacidity of the albumin microenvironment inside degrading microparticles from poly(lactide-co-glycolide) (PLG) or ABA-triblock polymers containing hydrophobic poly(lactide-co-glycolide) A blocks and hydrophilic poly(ethyleneoxide) B blocks, Pharm. Res. 15 (1998) 787–793.
[17] A. Brunner, K. Mader, A. Gopferich, pH and osmotic pressure inside biodegradable microspheres during erosion, Pharm. Res. 16 (1999) 847–853.
[18] P.A. Burke, Determination of internal pH in PLGA micropsheres using ^{31}P NMR spectroscopy, Int. Symp. Control. Bioact. Mater. 23 (1996) 133–134.
[19] J.C. Russ, The Image Processing Handbook, CRC Press, 1999.
[20] R.P. Haugland, Handbook of Fluorescent Probes and Research Products, Molecular Probes, 2002.
[21] G.Z. Zhu, S.P. Schwendeman, Stabilization of proteins encapsulated in cylindrical poly(lactide-co-glycolide) implants: mechanism of stabilization by basic additives, Pharm. Res. 17 (2000) 351–357.